On the Behaviour of Aluminium Foams under Uniaxial and Multiaxial Loading

W. Ehlers, H. Müllerschön & O. Klar
Institut für Mechanik (Bauwesen), Universität Stuttgart, Germany

Abstract

The present paper outlines the stress-strain behaviour of aluminum foams. To describe the response of the foam under arbitrary stress states, an elasto-plastic theory is used within the framework of the Theory of Porous Media (TPM). The goal of this paper is the identification of the parameters of the elasto-plastic model based on the results of uniaxial and multiaxial tests. For the examination of the elastic properties, uniaxial tests with unload-reload cycles are performed in order to isolate the reversible and hence the elastic part of the deformation. In contrast to the *von Mises*-like yield behaviour of pure aluminium, yielding of aluminium foam appears under isotropic compression as well as isotropic tension. This leads to a closed shape of the yield surface in the principal stress space. The triaxial compression tests and isotropic compression tests are carried out on cylindrical foam specimens to exhibit the dependence of the yielding behaviour on the hydrostatic stress state of the foam structure. Furthermore, biaxial tests (plane stress) are realized in order to obtain information about the shape of the yield curve in the deviatoric plane. The results of the uniaxial, triaxial and biaxial tests are the basis for an optimization process, whereby the yield criterion is adapted to the experimentally observed yield points by a least-squares objective function. The single-surface yield function used within the elasto-plastic model allows the decomposition in a hydrostatic and in a deviatoric part. Hence, a separate consideration of these two parts concerning the parameter identification is possible. A general requirement in the theory of plasticity is the constraint of convexity concerning the yield function. This leads to additional inequality constraints within the optimization process and hence to a constraint minimization problem. Therefore, the so called SQP-algorithm, which is based on a quadratic subproblem, is applied for the solution of the identification problem.

1 Material specification and geometry of the specimens

The aluminium foam is manufactured by *Hydro Aluminium a.s, R&D Materials Technology*. The foam consists of the alloy AlSi7Mg, with density in the range of $0.28\ \text{g/cm}^3 < \rho < 0.32\ \text{g/cm}^3$. This density corresponds to a porosity within the limits of $0.882 < n^F < 0.896$. The pore structure of the foam is approximately regular, apart from some anisotropic effects as a result of the foam growth direction. Nevertheless, pretests have shown, that the material behaviour of the foam is approximately isotropic.

J. Banhart, M.F. Ashby, N.A. Fleck: *Metal Foams and Porous Metal Structures.* © MIT Verlag (1999)

The samples are carefully prepared by sawing and, in case of the triaxial specimens by final turning. During this process damage of the pore structure at the surface of the samples should be avoided.

The geometry of the specimens and the definition of the applied load is shown in Figure 1.

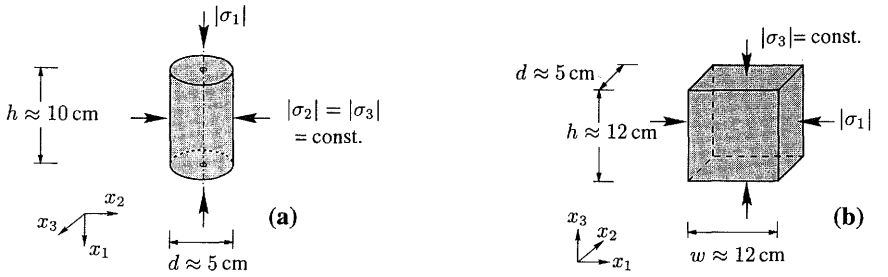

Figure 1: Sample geometry and definition of the applied loads for (a) triaxial testing and (b) biaxial testing

2 Elastic properties

Basis of the elasto-plastic theory is the assumption that the total deformation consists of the sum of a recoverable elastic part and an irreversible plastic part. Isolation of the elastic part from the total deformation within uniaxial compression tests is performed by unload-reload stress path, where approximately only recoverable strains occur. The slope of an unload-reload cycle in a stress-strain plot yields the parameter value for the *Young*'s modulus E_{ur}, see Figure 2. Thereby, a *Hooke*-type linear elasticity law is assumed.

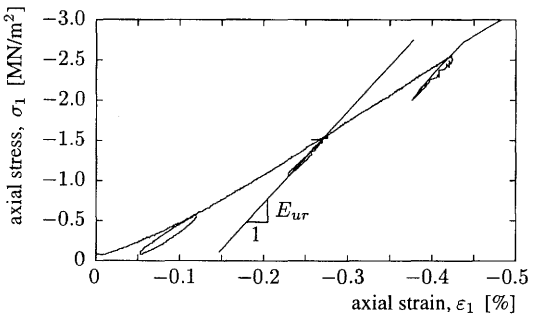

Figure 2: Determination of the *Young*'s modulus E_{ur} at the slope of an unload-reload cycle

It is very common to evaluate an initial *Young*'s modulus E_i as the slope of the linear strain curve before primary fracture occurs. In this range irreversible plastic strain portions are definitely included for the aluminium foam (Figure 2) and therefore, it is not suitable to determine elasticity constants in this way. In Figure 3 values of E_i evaluated for four different tests are plotted.

In addition, determination of the *Young*'s modulus is also carried out by acoustical methods [6], where measurement by resonance methods employing longitudinal and bending waves allows

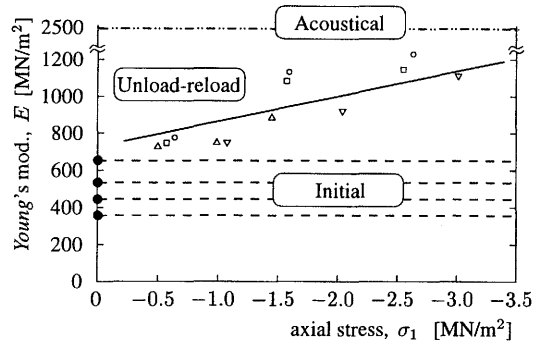

Figure 3: Values for the *Young*'s modulus of aluminium foam determined by three different methods

to draw conclusions regarding to the elastic properties. Figure 3 shows results for values of the *Young*'s modulus of aluminium foam evaluated by the above mentioned three different methods. For the mechanical tests, the values of σ_1 give the axial stress for which the unload-reload cycles are applied. Similar symbols belong to the same test. It is remarkable that the value for E carried out by acoustical methods is considerable higher than those obtained by mechanical methods. Experimental determination of *Poisson*'s ratio $\nu = -\varepsilon_3/\varepsilon_1$ is very difficult. Within the unload-reload cycles in the uniaxial compression tests, no significant deformation in the lateral direction ε_3 could be observed. Therefore, $\nu = 0$ is assumed.

3 Triaxial tests

Triaxial compression tests as well as isotropic compression tests are carried out on cylindrical foam specimens to exhibit the dependence of the yielding behaviour on the hydrostatic stress state of the foam structure.

3.1 Experimental set-up

Within the triaxial cell, the lateral load on the axisymmetric specimen is applied by the use of oil as a non-conductive medium (see Figure 4). Oil pressure is set by a hydraulic control unit. The load in axial direction is applied by a displacement driven press. Thereby, the axial strain is measured with a linear variable displacement transducer (LVDT) and the radial strain by a collar of two spring steel belts equiped with strain gages [7] (see Figure 4).

3.2 Results

A typical result of a triaxial compression test, for a constant lateral load of $\sigma_3 = -2.0$ MN/m^2, is plotted in Figure 5. At a specific point, a substantial drop of stress occurs due to fracture of complete foam-cell layers.
Compression tests for different values of σ_3 are performed as well as isotropic compression tests. The results of these tests give the input data for the adaption of the yield criterion in the hydrostatic plane.

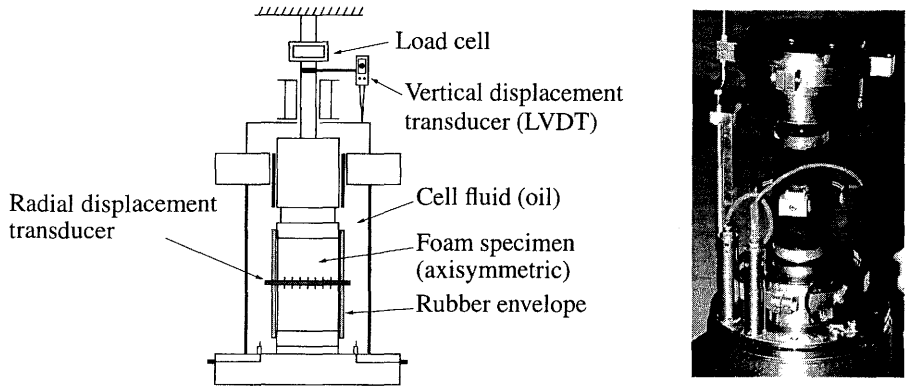

Figure 4: Diagrammatic layout of the hydraulic triaxial apparatus with a picture of the final set-up

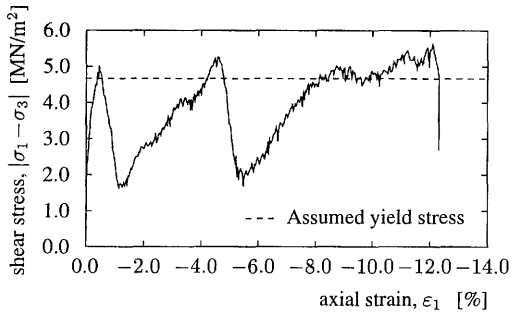

Figure 5: Result of a triaxial compression test with a constant lateral load of $\sigma_3 = -2.0$ MN/m^2

4 Biaxial tests

Biaxial tests (plane stress conditions) are performed in order to obtain information about the shape of the yield curve in the deviatoric plane. For these tests, a testing device is developed to realize large deformations in compliance with homogeneous deformation modes. At the interface between the specimen and the testing device, teflon layers are applied in order to reduce the friction during the deformation process (see Figure 6). The external load is applied under displacement control.

5 Modelling of plastic deformations

5.1 Yield criterion

As mentioned above, the well-known *von Mises*-yield criterion is not suitable for aluminium foam. Hence, a single-surface yield function is introduced with a closed shape of the yield contour in the principle stress space and a non-circular shape with respect to the deviatoric plane [2], see Figure 7.

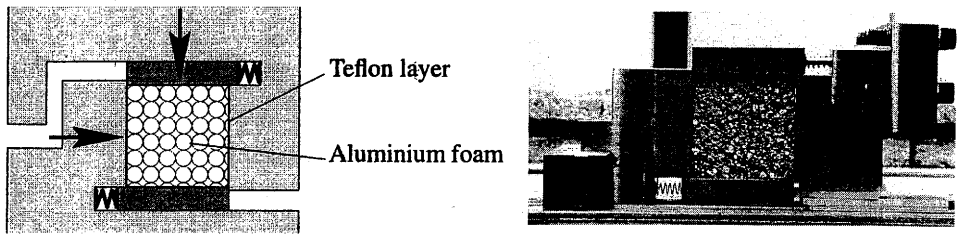

Figure 6: Experimental set-up of the biaxial test: layout and photography

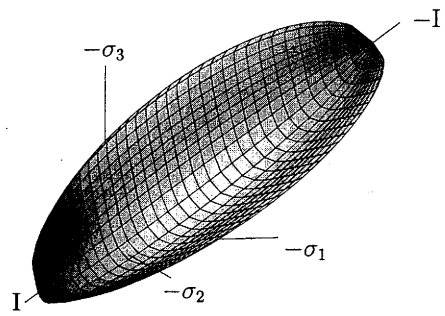

Figure 7: Geometrical representation of the yield function in the principle stress space

In the mathematical formulation of the yield function

$$F(\mathbf{T}, \boldsymbol{q}^h, \boldsymbol{q}^d) = \sqrt{\Gamma\, \mathrm{II}^D + \tfrac{1}{2}\alpha\, \mathrm{I}^2 + \delta^2\, \mathrm{I}^4} + \beta\, \mathrm{I} + \epsilon\, \mathrm{I}^2 - \kappa = 0\,,$$
$$\Gamma(\mathbf{T}, \boldsymbol{q}^d) = \left(1 + \gamma\, \mathrm{III}^D / (\mathrm{II}^D)^{3/2}\right)^m\,, \tag{1}$$

the invariants $\mathrm{I} = \mathbf{T} \cdot \mathbf{I}$, $\mathrm{II}^D = \frac{1}{2}\mathbf{T}^D \cdot \mathbf{T}^D$ and $\mathrm{III}^D = \frac{1}{3}\mathbf{T}^D \cdot (\mathbf{T}^D\,\mathbf{T}^D)$ of the stress tensor $\mathbf{T}$ characterize the stress state in (1). The additional index $(..)^D$ specifies the deviatoric part of the respective object; the symbol "$\cdot$" denotes the scalar product. The function $\Gamma(\mathbf{T}, \boldsymbol{q}^d)$ with the deviatoric parameter vector $\boldsymbol{q}^d = (\gamma, m)^T$ specifies the shape of the yield-curve in the deviatoric plane (cross-section perpendicular to the hydrostatic axis I, see Figure 7), the hydrostatic parameter vector $\boldsymbol{q}^h = (\alpha, \beta, \delta, \epsilon, \kappa)^T$ governs the shape of the yield curve in the hydrostatic plane (cross-section parallel to the hydrostatic axis I).
Reformulation of (1) using polar coordinates with the so-called *Reuß* variables

$$r = \sqrt{2\mathrm{II}^D} \quad \text{and} \quad \Theta = \frac{1}{3}\arcsin\left(\frac{\sqrt{27}}{2}\,\frac{\mathrm{III}^D}{(\mathrm{II}^D)^{3/2}}\right) \tag{2}$$

leads to

$$
\begin{aligned}
r(\Theta, \mathrm{I}) &= r^h(\mathrm{I})\, r^d(\Theta)\ , \\
r^h(\mathrm{I}) &= \sqrt{2}\left[(\epsilon^2 - \delta^2)\,\mathrm{I}^4 + 2\,\beta\,\epsilon\,\mathrm{I}^3 + + \left(\beta^2 - \tfrac{1}{2}\,\alpha - 2\,\epsilon\,\kappa\right)\mathrm{I}^2 - 2\,\beta\,\kappa\,\mathrm{I} + \kappa^2\right]^{1/2}\ , \qquad (3) \\
r^d(\Theta) &= \left[1 + \frac{2}{\sqrt{27}}\,\gamma\,\sin\left(3\,\Theta\right)\right]^{-m/2}\ .
\end{aligned}
$$

Therein, $r(\Theta, \mathrm{I})$ is the yield radius given as the product of two independent functions, $r^h(\mathrm{I})$ and $r^d(\Theta)$, where $r^h(\mathrm{I})$ represents the hydrostatic shape function while $r^d(\Theta)$ describes the shape of the yield criterion in the deviatoric plane (see Figure 7).
For more detailed information regarding to this section, it is referred to [1, 2, 4].

5.2 Parameter identification

In the uniaxial, triaxial and biaxial tests external load is increased up to those stress points where significant fracture occurs. These stress points are then assumed to be located on the yield or fracture surface in the principle stress space. To add information with respect to the tension range, uniaxial tensile tests, performed by partners of the EU-project METEOR, are incorporated in the parameter identification process (Figure 8).
The goal of the following optimization process is to minimize the distances of the experimentally observed yield points to the yield function (3) by variation of the parameter sets $\boldsymbol{q}^h$ and $\boldsymbol{q}^d$. Therefore, the identification procedure is based on the non-linear optimization problem

$$
\begin{aligned}
\Phi(\boldsymbol{q}) &= \tfrac{1}{2}\,\|R_m(\boldsymbol{q})\|_2^2 \quad \rightarrow \quad \min\,, \\
R_m(\boldsymbol{q}) &= r_m - r(\mathrm{I}_m, \Theta_m, \boldsymbol{q}) \qquad (4) \\
\boldsymbol{q} &= \boldsymbol{q}^h + \boldsymbol{q}^d\,.
\end{aligned}
$$

Here, m specifies the number of the experimental observations of the yield points concerning the yield radius r_m, the corresponding hydrostatic pressure I_m and the *Lode* angle Θ_m. The least-squares functional (4) is a function of the vector $\boldsymbol{q} \in \mathbf{R}^n$ which contains $n = 7$ material parameters involved in the yield criterion (3).
A general requirement in the theory of plasticity is the constraint of convexity concerning the yield function (principle of maximum dissipation [5]). This leads to additional inequality constraints governed by

$$
g^h(\boldsymbol{q}^h) = \frac{\partial^2 r^h(\mathrm{I})}{\partial \mathrm{I}^2} \leq 0 \qquad (5)
$$

for the hydrostatic part of the yield function and by

$$
g^d(\boldsymbol{q}^d) = (r^d)^2 + 2\left(\frac{\partial r^d}{\partial \Theta}\right)^2 - r^d\left(\frac{\partial^2 r^d}{\partial \Theta^2}\right) \geq 0 \qquad (6)
$$

for the deviatoric part [1]. Thus, the optimization process is concerned by a constraint minimization problem. Thereby, the considered inequality constraints (5) and (6) represent continous restrictions respective to I and Θ. Discretization of these continous constraints to a finite

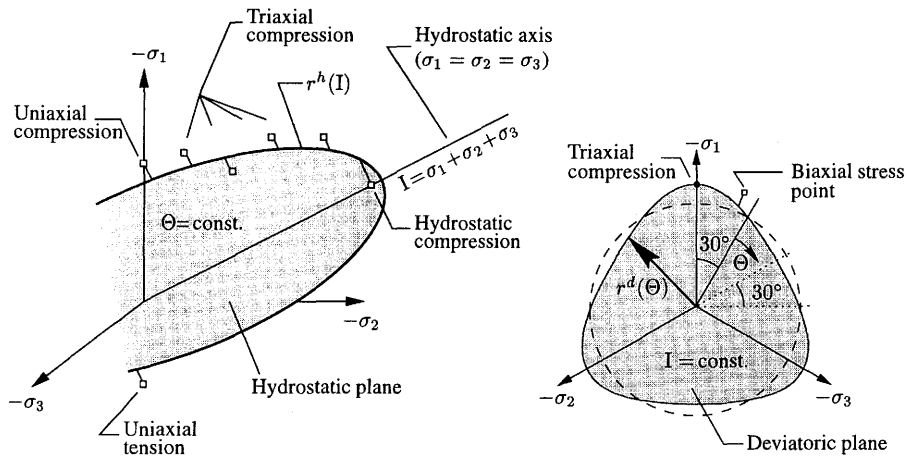

Figure 8: Geometrical interpretation of the distances between experimental points and the yield function which have to be minimized by the least-squares objective function (4)

number of inequality equations within the bounds of the yield function $r(\Theta, \mathrm{I})$ is necessary. The resulting constraints define the space of the admissible parameters. This leads to the problem

$$\Phi(\boldsymbol{q}) \rightarrow \min_{\boldsymbol{q}\in\Omega} \qquad \Omega = \left\{ \boldsymbol{q} \in \mathbf{R}^n : \boldsymbol{g}^h(\boldsymbol{q}^h) \geq 0 \in \mathbf{R}^{i^h}, \boldsymbol{g}^d(\boldsymbol{q}^d) \geq 0 \in \mathbf{R}^{i^d} \right\}, \tag{7}$$

where i^h and i^d denote the number of discrete inequality constraints. The constraint minimization problem (7) can be solved by the introduction of the *Lagrange* function $\mathcal{L}(\boldsymbol{q}, \boldsymbol{\lambda}) = \Phi(\boldsymbol{q}) + \boldsymbol{\lambda}^T \boldsymbol{g}$ with $\boldsymbol{g} = \boldsymbol{g}^h + \boldsymbol{g}^d$. By the consideration of the *Karush-Kuhn-Tucker* conditions $\partial\mathcal{L}/\partial\boldsymbol{q} = \mathbf{0}$, $\boldsymbol{\lambda} \geq 0, \boldsymbol{g} \leq 0$ and $\boldsymbol{\lambda}^T\boldsymbol{g} = 0$, a quadratic subproblem with linear constraints may be generated. On the basis of this quadratic subproblem the so-called SQP-algorithm is applied. Concerning the theory of SQP (Sequential Quadratic Programming) and nonlinear programming in general we refer to [8, 9].

In the present work we use the SQP-code "donlp2"[1] supplied by Prof. Spellucci (TU Darmstadt, Germany).

Results of the identification process for the parameters of the yield criterion are summarized in Table 1.

Parameter	α [-]	β [-]	γ [-]	δ [m^2/kN]	ϵ [m^2/kN]	κ [kN/m^2]	m [-]
Value	0.0196	0.07	1.40	$1.76 \cdot 10^{-5}$	$1.96 \cdot 10^{-6}$	2020	0.61

Table 1: Parameter values $\boldsymbol{q}$ of the yield criterion calculated by the minimization problem (7)

[1] donlp2-programme and users guide are available from www.netlib.org/opt

6 Conclusions

In the present work, the evaluation of a mechanical correct *Young*'s modulus within unload-reload loops in uniaxial tests is demonstrated. Furthermore, the experimental set-up for triaxial tests as well as for biaxial tests is shown. By the results of these multiaxial tests, the parameter identification for the three-dimensional yield surface in the principle stress space is applied. The results of the parameter evaluation concerning the reversible (elastic) and irreversible (plastic) material behaviour may be used for the elasto-plastic model described in [1, 3, 4].

Acknowledgements

The research work has been carried out within the framework of the European Commission's "Industrial and Materials Technologies" (Brite EuRam III) multiannual (94-98) programme for R & D. The authors gratefully acknowledge the collaboration of all partners of the METEOR project "Light-weight Metal Foam Components for the Transport Industry" (Contract BRPR-CT96-0215, project BE96-3018).
The multiaxial experiments are performed in cooperation with the Institut für Bodenmechanik und Felsmechanik, Universität Karlsruhe (TH). The authors would like to thank for the effective cooperation.

References

[1] W. Ehlers, Continuum Mechanics in Environmental Sciences and Geophysics, CISM Courses and Lectures Notes No. 337, Ed: K. Hutter, Springer-Verlag, Berlin (1993), p. 313

[2] W. Ehlers, Arch. Appl. Mech. 63, 65 (1995)

[3] W. Ehlers, A. Droste, ZAMM 79 (in press), (1999)

[4] W. Ehlers, H. Müllerschön, On Coupled Solid Fluid Problems for Cohesionless Soils. In: Vitharana N and Colman R (ed): Proc. of 8th Australian New Zealand Conference on Geomechanics, Eds: N. Vitharana, R. Colman, Vol. 2, Hobart-Tasmania (1999), p. 945

[5] R. Hill, *The Mathematical Theory of Plasticity*, Oxford University Press, Oxford (1950)

[6] F. G. Kollmann, *Maschinenakustik*, Springer Verlag, Berlin (1993)

[7] D. Kolymbas, W. Wu, Geotech. Test. J. 3, Vol. 12, 227 (1989)

[8] D. G. Luenberger, *Linear and Nonlinear Programming*, Addison-Wesley Publishing, Reading-Massachusetts (1984)

[9] P. Spellucci, *Numerische Verfahren der nichtlinearen Optimierung*, Birkhäuser, Basel (1993)